

Tip-induced deformation of polystyrene latex reference nanoparticles in atomic force microscopy

Natalia Farkas^{1,2,a)} and John A. Kramar²

¹Theiss Research, 7411 Eads Ave, La Jolla, CA 92037

²National Institute of Standards and Technology, Gaithersburg, MD 20899

a) Electronic mail: natalia.farkas@nist.gov

The measurement approach typically prescribed for sizing polystyrene latex (PSL) reference nanoparticles by atomic force microscopy (AFM) is based on a single value of the height obtained from a three-dimensional image of the particle. A major challenge is that PSLs reportedly deform during sample preparation as well as imaging. While the particle-substrate deformation is controlled by adhesive contact forces, the tip-induced deformation may vary to a large degree depending on the operational conditions and the geometrical constraints imposed by the instrument. In this paper, we are mainly concerned with the effect of cantilever tilt, tip shape and setpoint voltage on tip-induced deformation of PSL reference nanoparticles. Tips are characterized by scanning electron microscopy and using a multilayer Si/SiO₂ tip characterizer. We find that the plastic flow of materials, induced by the asymmetric imaging geometry, shifts the position of the maximum particle height away from the center. This shape-change often leads to an initial height increase for PSLs that are smaller than 40 nm. Since AFM height analysis algorithms often equate apparent particle height with the highest measured point of the particle, these results have implications from the perspective of AFM-based nanoparticle metrology.

I. INTRODUCTION

Polystyrene latex (PSL) spheres are one of the most important particle reference materials for ensuring measurement accuracy and traceability at the nanoscale in many metrological and research-oriented applications. PSLs have for decades been invaluable for calibration of particle sizing instruments and validation of commercial test materials [1,2,3] due to nearly ideal properties, i.e., sphericity and monodispersity, and inexpensive commercial production. Representative images of nominally 100 nm diameter PSL nanoparticles are shown in Fig. 1.

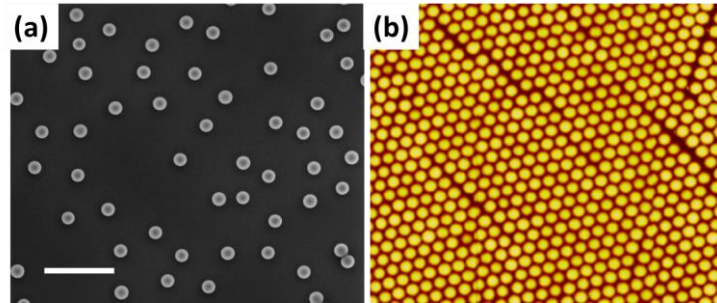


FIG. 1. Images of nominally 100 nm diameter PSL nanoparticles. The SEM (a) and AFM (b) images correspond to individual and close-packed raft particles, respectively. The common scale bar is 500 nm.

Size measurement of such spherical nanoparticles are either based on the height of individual particles or on a line average obtained from a two-dimensional array of close-packed particles. Recently however, numerous studies have encountered particle deformation in both methods [4,5,6]. Adhesive contact-deformation to a substrate or neighboring particles occurs during sample preparation, while tip-induced deformation may arise during imaging. These contributions were methodically considered in our previous work [7] by the use of a statistical error-correction function developed based on

analysis of correlated AFM height and width measurements of individual PSLs. Although we thoroughly investigated the deformation response of PSL nanoparticles to AFM tapping forces under different setpoint voltages, we limited our focus on tip-induced deformation that was minimal and elastic. In this paper, we discuss tip-induced deformation of PSL nanoparticles in the plastic regime and investigate the effect of the AFM cantilever tilt and tip geometry on the plastic flow of materials under hard tapping.

II. EXPERIMENTAL

A. Reference nanoparticles

SRM 1964, a polystyrene latex (PSL) nanoparticle sample with certified size of 60.39 nm [8], was obtained from the National Institute of Standards and Technology. The size, i.e. the spherical-equivalent-volume diameter, of the particles in the sample ranges from 20 nm to 65 nm. PSL nanoparticles were attached to a poly-L-lysine coated mica substrate for AFM imaging. The substrate was prepared by incubating a freshly cleaved mica substrate with 0.01 % poly-L-lysine for 10 minutes. The substrate was then blown dry with high-purity compressed air. A 50 μ L drop of diluted nanoparticle solution was incubated on the substrate for 5 minutes, rinsed with DI water, and any remaining solvent removed by gently blowing with air.

B. Atomic force microscopy

A Veeco MultiMode AFM with Nanoscope IV controller, series J scanner, and v.6 software was used for imaging and particle size analysis [9]. A first-order image flattening routine was applied to obtain a global background suitable for obtaining

particle height measurements. Imaging was performed in TappingMode using Bruker OTESPA ($k = 42 \text{ N/m}$) silicon tips. An initial setpoint voltage was established at 85% of the 2 V drive voltage. Optimized tapping-mode AFM operating conditions were established by monitoring topography, phase angle, and amplitude channels during imaging. The microscope was shielded from air currents in a hood and the room was maintained under constant temperature and relative humidity, $(23 \pm 0.5) \text{ }^\circ\text{C}$ and $(28 \pm 8) \%$ RH, respectively. AFM scanner calibration of the lateral fast-scan, or X axis direction, was performed using a 70-nm pitch standard grating [10]. Calibration of the height, or Z axis, was performed using a set of NANO2 step height reference standards over the range of 7 nm to 700 nm [11]. The expanded uncertainty calculated at the 95 % confidence interval for the AFM height measurements is 1.6 nm. In addition to repeatability of replicate measurements, other major uncertainty components arise from background flatness, instrument noise, and calibration. The combined standard uncertainty is estimated as the square root of the sum of the squares of the individual uncertainty components.

C. Scanning electron microscopy

An FEI Helios Dual-Beam SEM was used to image the OTESPA tips. Imaging was carried out on uncoated samples. A working distance of 4 mm, accelerating voltage of 5 keV, and beam current of 43 pA were used to obtain all images. The magnification of the instrument was calibrated using a traceable 100-nm grating sample.

III. RESULTS AND DISCUSSION

A. Interaction between tip and particle

In tapping-mode AFM, the setpoint voltage maintains the oscillation amplitude of the integrated tip and cantilever and indirectly controls the imaging force it applies to the sample. The lower the setpoint voltage, the larger the applied force. Such interaction between the tip and the nanoparticles may impact the outcome of AFM size measurements. In our previous work, we concluded that it was possible to realize a zero-deformation condition for tapping-mode imaging of PSLs only if the setpoint voltage remains within a narrow operating range around the optimal value and repeated scanning is avoided [7].

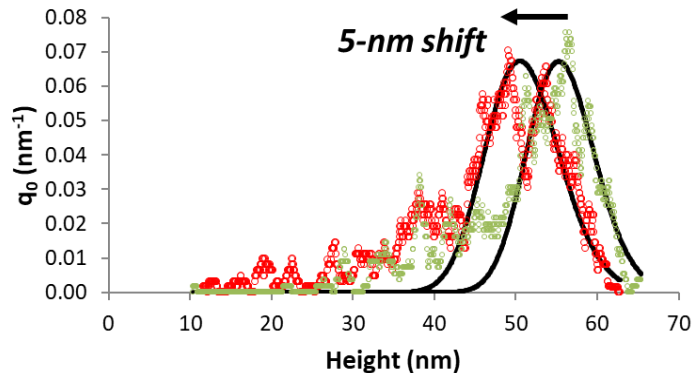


FIG. 2. Number-weighted density distribution functions obtained by AFM for SRM 1964 at zero-deformation setpoint (right) and under hard tapping (left). The solid lines are lognormal fits to the distributions. The arrow indicates a shift in the modal height value.

In contrast, if the setpoint voltage is adjusted to too low a value (hard tapping), PSL nanoparticles deform significantly after even a single scan. We show this in Fig. 2 where particle size measurements of SRM 1964 obtained at the optimal, zero-deformation setpoint and under hard tapping are compared. In the latter case, the tip-

induced deformation results in an underestimation of the modal height value of the PSL nanoparticles by 10 %. The results demonstrate that improper choice of setpoint voltages could easily induce deformation greater than the 3.4-nm contact-deformation determined in our previous study [7]. To avoid such significant measurement error, an optimal setpoint voltage must be determined for each specific AFM tip, and its stability monitored and maintained through deliberate electromechanical process control during image acquisition.

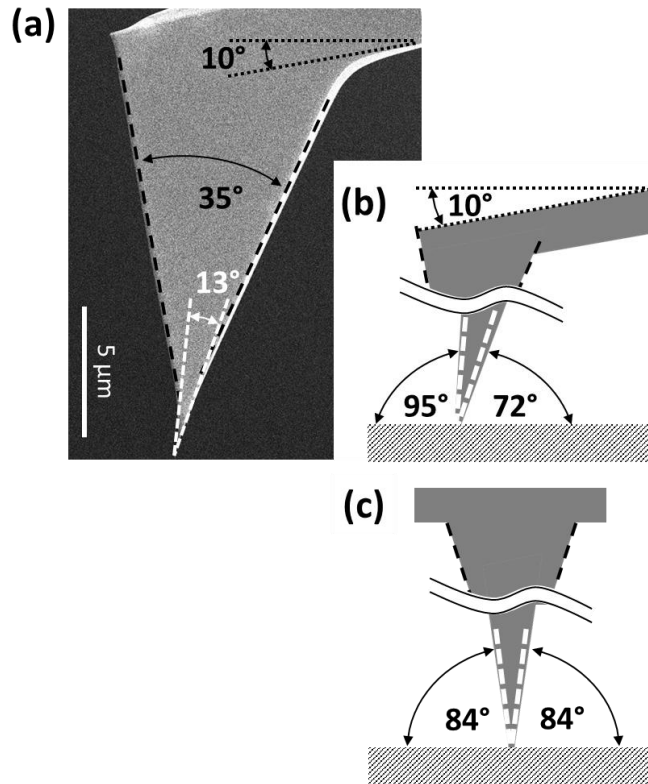


FIG. 3. (a) SEM image of an OTESPA tetrahedral silicon tip in the front-to-back direction. (b) and (c) Orientation angles of the tip with respect to a horizontal sample surface in the front-to-back and side-to-side directions, respectively.

In addition, the AFM cantilever is commonly orientated at a small, i.e., 10° to 15° , angle to the surface, which is necessary to avoid contact of the AFM tip holder with the sample. Fig. 3 shows the geometry of a tetrahedral silicon AFM tip (OTESPA) used in this study. The tip profile in the front-to-back scanning direction differs from that in the side-to-side scanning direction. Here, front-to-back (side-to-side) refers to the tip geometry parallel (perpendicular) to the major axis of the cantilever. The tip is asymmetric with a nominal 35° tip angle, and a 10° tip holder tilt in the front-to-back direction as indicated in the SEM image shown in Fig. 3a. Note that the SEM image represents a view of the tip and cantilever along the long cantilever axis which is the orientation typically used for routine imaging and referred to as the front-to-back direction in this work. The SEM image also shows that oxide sharpening of the apex significantly reduces the tip angle (Fig. 3a) and alters its scanning geometry with respect to the surface (Fig. 3b). The tip is symmetric in the side-to-side direction with a nominal 35° tip angle that narrows down to about 12° with the oxide sharpening process.

The cantilever tilt increases the complexity of the interaction between the tip and particle, and results in a tangential force applied by the AFM tip that is not directed symmetrically onto the curved particle surface. Several studies have been conducted to quantify the influence of the AFM cantilever tilt on the geometry and mechanism of force measurements [12,13,14]. Through theoretical calculations as well as experiments, they show that the tilt induces torque and changes the effective spring constant. AFM deformation studies of PSLs, on the other hand, are generally concerned with the measurement of only the particle height change without much consideration of the three-dimensional aspects of the problem. The next section explores—for the first time—the

effect of the AFM cantilever tilt and tip geometry on the tip-induced deformation and plastic flow of materials under hard tapping.

B. Plastic deformation

By acquiring a sequence of particle cross-sections from AFM images in which the setpoint voltage is reduced from its optimal to increasingly smaller values, we observe that the PSLs exhibit significant deformation at reduced setpoint voltages (Fig. 4). Signs of deformation appear as the set point voltage diverges increasingly from optimal imaging conditions (Fig. 4a and 4b). Comparison of the particle cross sections in Fig. 4c and 4d suggests that flattening of the particles appears asymmetric and symmetric in the front-to-back and side-to-side direction, respectively. In side-to-side scanning the applied force of the AFM tip is directed symmetrically onto the curved particle surface. However, during front-to-back scanning the applied force of the AFM tip is not directed symmetrically onto the curved particle surface because of the characteristics of the cantilever and the tip geometry shown in Fig. 3. As the number of scans increases, the material flow induced by low setpoint operation accompanied by considerable lateral forces in this case leads to asymmetric shapes of the compressed PSLs. The plastic deformation is cumulative and continuously shifts the position of the maximum particle height away from the center as indicated by the arrow in Fig. 4b and 4c.

Our results are closely parallel to those found in the work reported by Zhang et al. [15] where a connection was established between plastic deformation of polystyrene (PS) and a glass-to-rubber transition under AFM tapping mode conditions. In their study, PS nanostructures, 100 nm in diameter, are phase separated and geometrically confined by a

matrix of poly(methyl methacrylate) (PMMA). The morphology of the deformation they observed was the formation of a shoulder along the edges of the PS nanostructures with simultaneous depression of the inner PS regions when scanning at reduced tapping mode setpoint voltages. In the case of these PS nanostructures as well as the spherical PSL nanoparticles in this study (Fig. 4c and 4d), the deformation is due to material flow that is cumulative throughout repeated scans under hard tapping conditions. The response of the asymmetric AFM tip geometry in the front-to-back direction is reflected in an elongation of the original particle/nanostructure shape as shown in Fig. 4b and Fig. S3 of ref. 15.

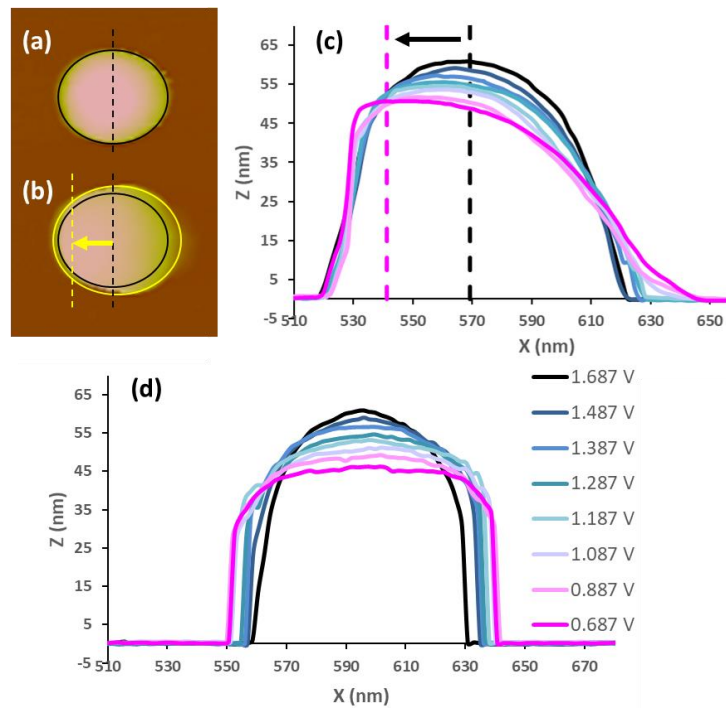


FIG. 4. AFM images of a selected PSL nanoparticle acquired (a) at zero-deformation setpoint and (b) after scanning with increasingly smaller setpoint voltages. Sequence of particle cross-sections in the (c) front-to-back and (d) side-to-side directions. Dashed lines indicate the location of the maximum height values of the particle at the beginning and the end of the imaging sequence, and the arrows show the shift between them.

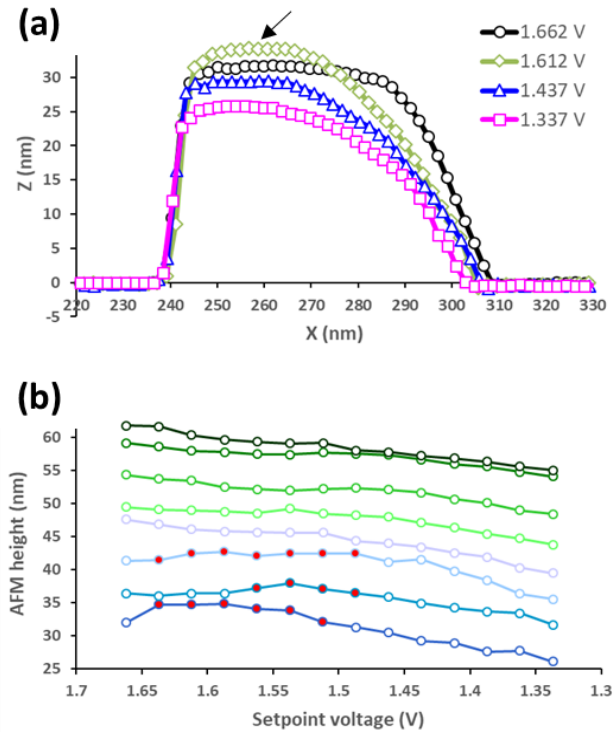


FIG. 5. (a) AFM cross sections of a 30-nm PSL nanoparticle obtained at increasingly-lower setpoint voltages. The arrow indicates the occurrence of a shape-change related height increase. (b) AFM height vs. setpoint voltage for PSLs in the 30 nm to 60 nm size range. Red data points indicate height values that are larger than the original particle heights acquired under zero-deformation conditions.

We also find that the asymmetric AFM tip geometry in the front-to-back direction may lead to material flow and asymmetric shape changes such that the particle height may increase, as opposed to decrease, as the result of the deformation. This effect—which is more likely to occur the smaller the particles are—is illustrated in Fig. 5a and 5b. These results also explain a recently reported—and seemingly anomalous—observation of an apparent height increase in AFM imaging of small (20-50) nm PSL nanoparticles [6]. The size measurement of spherical nanoparticles by AFM is typically

based on a single height value obtained from a three-dimensional image of the particle [1,2]. The consequence is that almost all information about the particle is left unused. A closer look at Fig. 4 and 5 reveals that, as the setpoint voltage is reduced, the asymmetric material flow shifts and, in some cases, increases the maximum height value along the front-to-back scanning direction. Because AFM height analysis algorithms often equate apparent particle height with the highest measured point of the particle, the three-dimensional nature of the deformation likely leads to an increased particle height, especially in the aforesaid small size range.

C. *Asymmetric tip wear*

The cantilever tilt also affects tip wear. In Fig. 6, high-resolution SEM images of a new (Fig. 6a and 6b) and an extensively used tip (Fig. 6c) are aligned and overlaid with additional intervening reconstructed tip-shape profiles. The tip characterization process, shown in Fig. 7a in the front-to-back and side-to-side imaging directions, includes combined measurements of a knife edge and a series of rectangular trench structures of several widths (Fig. 7b) on a Si/SiO₂ tip characterizer [16,17]. The knife edge structure is used to reconstruct tip profiles from cross-sectional segments that are inverted in both horizontal and vertical directions as indicated in Fig. 7c and 7d. The tip penetration depths (D) are also measured and combined with the respective width of the trenches (W) to obtain several corroborating data points on the tip profile.

Tip wear tests shown in Fig. 6 were done under hard tapping, i.e. using substantially-lower-than-normal operating setpoint voltages, for accelerated wear conditions. Visualization of tip change due to wear suggests that the back (right) side of

the tip coincides with the original tip profile while the front (left) side of the tip originates from fracture/wear. Silicon AFM tips are expected to fracture during the initial and conceivably during subsequent engagement of feedback control, which effectively determines the tip shape [18]. Alignment of the reconstructed tip shapes to the SEM images in Fig. 6a and 6c indicates that tips generally retain a characteristic geometry in the front-to-back imaging direction. In particular, the fracture lines tend to create a front angle that is similar to the back angle. This is how nearly symmetrical cross-sections (Fig. 4c) may be obtained for spherical PSLs under zero-deformation conditions despite the seemingly asymmetric tip/cantilever geometry shown in Fig. 3 for the front-to-back imaging direction.

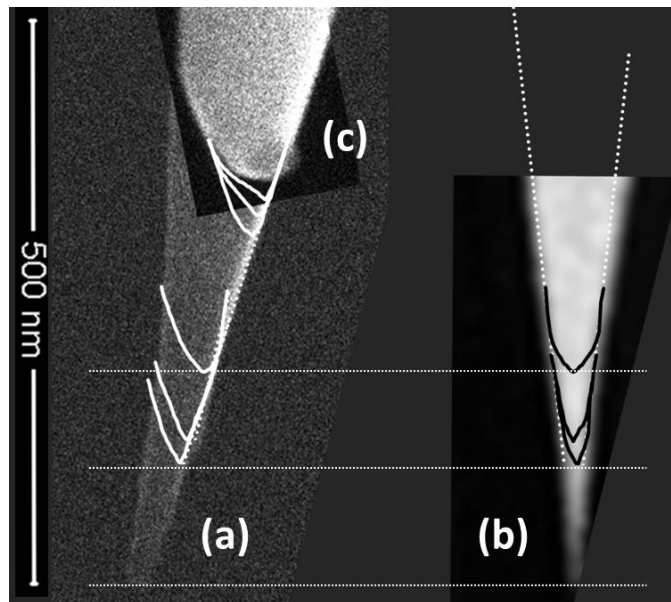


FIG. 6. (a) SEM images of a new tip in the front-to-back direction. (b) SEM image of a new tip in the side-to-side direction. Image courtesy of Olympus Corporation [19]. (c) SEM image of an excessively worn tip. Reconstructed AFM tip profiles obtained using the Si/SiO₂ tip characterizer are superimposed onto the SEM images in both directions. Corresponding front-to-back and side-to-side tip shapes are indicated by horizontal lines.

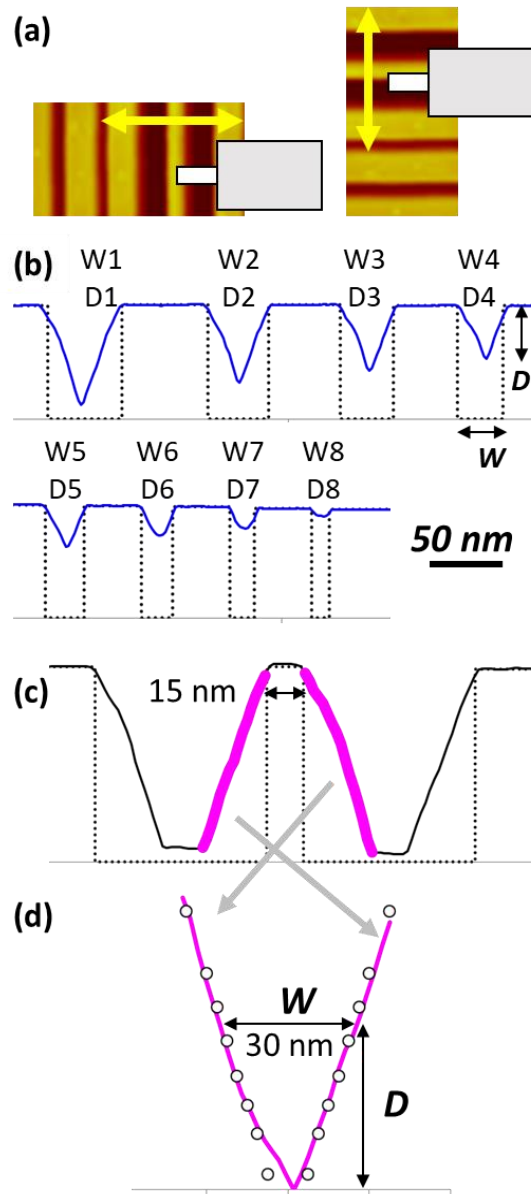


FIG. 7. (a) Schematic of tip characterization in the front-to-back and side-to-side imaging directions using multilayer Si/SiO₂ structures. AFM line scan of (b) a series of rectangular trenches and (c) a knife edge structure. (d) Reconstructed OTESPA tip profile (solid line) and W , D data pairs (circles) obtained from cross-sectional analysis of the trenches.

IV. SUMMARY AND CONCLUSIONS

The key purpose of the work was to investigate an important, but often neglected consideration in the interpretation of AFM deformation measurements of compressible nanoparticles, that is, the inherently three-dimensional nature of the imaging geometry. The results presented here show that the cantilever tilt and tip geometry significantly affect the measured height and shape of PSL reference nanoparticles under hard tapping conditions. The effective orientation of the tip with respect to the surface—which is markedly different in the front-to-back and side-to-side imaging directions, as revealed by SEM—induces directionality in the plastic deformation of PSLs and leads to asymmetric tip wear as well. The deformation is cumulatively asymmetric in the front-to-back scanning direction, and the plastic flow of the material shifts the location of the highest measured point on the particle to off-center. The observed shape-change explains previous ambiguities in AFM height measurements of compressible PSL nanoparticles, especially in the less-than 40 nm size range.

ACKNOWLEDGMENTS

The authors wish to thank András E. Vladár (NIST) and Prem Kavuri (NIST) for their assistance with SEM imaging. The authors also acknowledge insightful discussions with John A. Dagata (NIST) and Chung-Lin Wu (ITRI).

REFERENCES

¹M. Kitajima and Y. Fukai, *Colloids Surf., A* 153, 467 (1999).

²B. Y. H. Liu, F. J. Romay, W. D. Dick, K.-S. Woo, and M. Chiruta, *Aerosol Air Qual. Res.* 10, 125 (2010).

³G. W. Mulholland and B. J. Bauer, *J. Nanopart. Res.* 2, 5 (2000).

⁴J. Garnaes, *Meas. Sci. Technol.* 22, 094001 (2011).

⁵B-C. He, W-E. Fu, H-C. Liou, S-P. Pan, H-M. Lin, and Y-F. Chen, *Proc. SPIE* 8378 83780G (2012).

⁶B. Babic, M. A. Lawn, V. A. Coleman, Å. K. Jämting, and J. Herrmann, *J. Appl. Phys.* 119, 214307 (2016).

⁷J. A. Dagata, N. Farkas, P. Kavuri, A. E. Vladar, C.-L. Wu, H. Itoh, and K. Ehara, *NIST Spec. Publ.* 260, 185 (July 2016).

⁸NIST SRM 1964 Certificate of Analysis (2007).

⁹Certain commercial equipment, instruments, or materials are identified in this paper in order to adequately specify the experimental procedure. Such identification does not imply recommendation or endorsement by NIST, nor does it imply that the materials or equipment identified are necessary the best available for the purpose.

¹⁰R. Dixson, D. A. Chernoff, S. Wang, T. V. Vorburger, S.-L. Tan, N. G. Orji, and J. Fu, *J. Micro/Nanolithogr. MEMS MOEMS* 10, 013015 (2011).

¹¹L. Koenders, et al., *Metrologia* 40, 04001 (2003).

¹²L.-O. Heim, M. Kappl, and H.-J. Butt, *Langmuir* 20, 2760 (2004).

¹³S. A. Edwards, W. A. Ducker, and J. E. Sader, *J. Appl. Phys.* 103, 064513 (2008).

¹⁴R. S. Gates, *Rev. Sci. Instrum.* 88, 123710 (2017).

¹⁵H. Zhang, Y. Honda, and S. Takeoka, *Langmuir* 29, 1333 (2013).

¹⁶H. Itoh, T. Fujimoto, and S. Ichimura, *Rev. Sci. Instrum.* 77, 103704 (2006).

¹⁷H. Takenaka, M. Hatayama, H. Ito, T. Ohchi, A. Takano, and S. Kurosawa, *e-J. Surf. Sci. Nanotechnol.* 9, 293 (2011).

¹⁸K.-H. Chung, Y.-H. Lee, and D.-E. Kim, Characteristics of fracture during the approach and wear mechanism of a silicon AFM tip, *Ultramicroscopy* 102, 161 (2005).

¹⁹<http://probe.olympus-global.com/en/product/scanprfl.html#apex>

BIOGRAPHIES



Dr. Natalia Farkas is a Research Scientist with Theiss Research and an Associate in the Nanoscale and Nanostructure Metrology Group at the National Institute of Standards and Technology. She received a PhD degree in Physical Chemistry from the University of Akron. Her doctoral research, for which she received the AVS Nellie Yeoh Whetten Award in 2005, concerned the development of novel materials and methods for lithographic patterning of nanometer-scale structures. A substantial part of her experimental work was performed at NIST. Her internship experience there was career-changing from both a personal and a scientific perspective. Her objective had been to pursue teaching in academia until she experienced the investigative excitement of pursuing pure research. Taking part in challenging and rewarding research at NIST, she developed a great interest in

measurement science and was inspired to conduct further research in the fields of physical chemistry and nanotechnology, including scanning probe microscopy and its use in dimensional metrology and biomedicine. Following the receipt of the PhD degree in 2006, she returned to NIST as a full-time Associate researcher. Her work there has focused on pre-clinical dimensional and analytical chemical characterization of self-assembled nanoparticle delivery systems having encapsulated gene therapy and magnetic resonance imaging contrast agents, and, most recently, on the development of validated multi-technique measurement methods for the standardization of nanoparticle reference materials.



Dr. John Kramar is Leader of the Nanoscale and Nanostructure Metrology Group at the National Institute of Standards and Technology (NIST). Dr. Kramar earned a Ph.D. in Chemistry from the California Institute of Technology, where his thesis subject was scanning tunneling microscopy and spectroscopy of molybdenum disulfide. In 1990 he joined NIST to work on the Molecular Measuring Machine Project. His current research interests are in length and size nanometrology and its applications, including standards and methodology development for nanoparticle size, shape, distribution, count, composition and internal structure measurements.

FIGURE CAPTIONS

FIG. 1. Images of nominally 100 nm diameter PSL nanoparticles. The SEM (a) and AFM (b) images correspond to individual and close-packed raft particles, respectively. The common scale bar is 500 nm.

FIG. 2. Number-weighted density distribution functions obtained by AFM for SRM 1964 at zero-deformation setpoint (right) and under hard tapping (left). The solid lines are lognormal fits to the distributions. The arrow indicates a shift in the modal height value.

FIG. 3. (a) SEM image of an OTESPA tetrahedral silicon tip in the front-to-back direction. (b) and (c) Orientation angles of the tip with respect to a horizontal sample surface in the front-to-back and side-to-side directions, respectively.

FIG. 4. AFM images of a selected PSL nanoparticle acquired (a) at zero-deformation setpoint and (b) after scanning with increasingly smaller setpoint voltages. Sequence of particle cross-sections in the (c) front-to-back and (d) side-to-side directions. Dashed lines indicate the location of the maximum height values of the particle at the beginning and the end of the imaging sequence, and the arrows show the shift between them.

FIG. 5. (a) AFM cross sections of a 30-nm PSL nanoparticle obtained at increasingly-lower setpoint voltages. The arrow indicates the occurrence of a shape-change related height increase. (b) AFM height vs. setpoint voltage for PSLs in the 30 nm to 60 nm size range. Red data points indicate height values that are larger than the original particle heights acquired under zero-deformation conditions.

FIG. 6. (a) SEM images of a new tip in the front-to-back direction. (b) SEM image of a new tip in the side-to-side direction. Image courtesy of Olympus Corporation [19]. (c)

SEM image of an excessively worn tip. Reconstructed AFM tip profiles obtained using the Si/SiO₂ tip characterizer are superimposed onto the SEM images in both directions. Corresponding front-to-back and side-to-side tip shapes are indicated by horizontal lines.

FIG. 7. (a) Schematic of tip characterization in the front-to-back and side-to-side imaging directions using multilayer Si/SiO₂ structures. AFM line scan of (b) a series of rectangular trenches and (c) a knife edge structure. (d) Reconstructed OTESPA tip profile (solid line) and W, D data pairs (circles) obtained from cross-sectional analysis of the trenches.